Journal of Physics and Chemistry of Solids 74 (2013) 1533–1537

Contents lists available at SciVerse ScienceDirect

Journal of Physics and Chemistry of Solids

journal homepage: www.elsevier.com/locate/jpcs

Near infrared to UV dielectric functions of Al doped ZnO films deposited on *c*-plane sapphire substrate using pulsed laser deposition

R. Thangavel [a,b,c,*], Mohammad Tariq Yaseen [b,d], Yia Chung Chang [b,c], Chia-Hao Hsu [e], Kuo-Wei Yeh [e], Maw Kuen Wu [e]

[a] Department of Applied Physics, Indian School of Mines, Dhanbad 826004, India
[b] Research Centre for Applied Sciences, Academia Sinica, Taipei, Taiwan 115, Republic of China
[c] Department of Photonics, College of Electrical and Computer Engineering, National Chiao Tung University, Hsinchu, Taiwan 300, Republic of China
[d] Department of Engineering and System Science, National Tsing Hua University, Hsinchu, Taiwan, Republic of China
[e] Institute of Physics, Academia Sinica, Taipei, Taiwan 115, Republic of China

ARTICLE INFO

Article history:
Received 16 January 2013
Received in revised form
2 April 2013
Accepted 15 May 2013
Available online 4 June 2013

Keywords:
A. Thin films
C. Raman spectroscopy
C. X-ray diffraction
D. Electrical properties
D. Optical properties

ABSTRACT

Transparent conducting polycrystalline Al-doped ZnO (AZO) films were deposited on sapphire substrates at substrate temperatures ranging from 200 to 300 °C by pulsed laser deposition (PLD). X-ray diffraction measurement shows that the crystalline quality of AZO films was improved with increased substrate temperature. The electrical and optical properties of the AZO films have been systematically studied via various experimental tools. The room-temperature micro-photoluminescence (μ-PL) spectra show a strong ultraviolet (UV) excitonic emission and weak deep-level emission, which indicate low structural defects in the films. A Raman shift of about 11 cm^{-1} is observed for the first-order longitudinal-optical (LO) phonon peak for AZO films when compared to the LO phonon peak of bulk ZnO. The Raman spectra obtained with UV resonant excitation at room temperature show multi-phonon LO modes up to third order. Optical response due to free electrons of the AZO films was characterized in the photon energy range from 0.6 to 6.5 eV by spectroscopic ellipsometry (SE). The free electron response was expressed by a simple Drude model combined with the Cauchy model are reported.

1. Introduction

Transparent conducting oxide (TCO) films have been widely used for mobile display applications, such as organic light-emitting diodes, liquid crystal displays (LCDs), micro displays, and solar cells [1]. In most cases, indium tin oxide (ITO) has been widely employed as a TCO material because of its superb electrical and optical properties. However, ITO has low stability, high toxicity, and high cost and is a rare material, which is a motivating factor to develop alternatives [2,3]. In particular, ZnO film doped with Al, an n-type dopant, has attracted attention as TCO because of its low resistance and high transparency to visible lights. ZnO-based TCOs are relatively inexpensive and they also have desirable properties such as nontoxicity, long-term environmental stability and excellent IR shielding [4,5]. Recent research reveals that Al, B and Ga doped ZnO films show low resistivity and high transparency [6–8]. There are several deposition techniques which have been used to grow AZO thin films, including chemical vapor deposition (CVD), [9,10] magnetron sputtering, [11–13] spray pyrolysis, [14,15] and pulsed-laser deposition (PLD) [16,17]. In comparison with other techniques, PLD provides several advantages. The composition of the films grown by PLD is quite close to that of the target, even for multicomponent targets. PLD films crystallize at lower substrate temperatures due to the high kinetic energies (>1 eV) of the atoms and ionized species in the laser-produced plasma [18]. Also, the surface of the films grown by PLD can be very smooth [19]. For some product applications, the TCO must be synthesized at a temperature under 300 °C [20].

Optical measurements have been carried out to measure refractive indices and absorption coefficients for AZO films in the past [21–25]. The spectroscopic ellipsometry (SE) can provide a precise and more informative measurement. By measuring the ratio of light reflected off the surface of the film for two polarization states (i.e., TM and TE modes) and subsequently utilizing an appropriate dispersion model, one can extract both the real and imaginary parts of the dielectric function directly without involving Kramers–Kronig (K–K) analysis. In addition, the film thickness can also be determined precisely. Spectroscopic ellipsometry has been recently used to determine the optical functions of ZnO films [26–31]. But up to now, very few studies have been reported to

* Corresponding author at: Indian School of Mines Dhanbad 826004, Department of Applied Physics, Dhanabd 826004, India. Tel.: +91 326 223 5916; fax: +91 326 229 6563.
E-mail address: rthangavel@gmail.com (R. Thangavel).

0022-3697/$ - see front matter © 2013 Elsevier Ltd. All rights reserved.
http://dx.doi.org/10.1016/j.jpcs.2013.05.020

extract the optical constants of AZO films by spectroscopic ellipsometry. Here, we have used a sub-molecular doping technique for preparing the Al-doped ZnO films. The main focus is to determine the optical constants and band gaps of the AZO films using spectroscopic ellipsometry at room temperature.

In this paper, the Raman spectra were studied in detail, and a new vibrational mode at 498 cm^{-1} was observed in the Raman spectra of the AZO films. To the best of our knowledge, the vibrational mode assigned at 498 cm^{-1}, which results from the Al doping, has not been reported anywhere. The optical response due to free electrons of the AZO films was characterized by spectroscopic ellipsometry (SE). From the results of the SE analysis and the Hall measurements, electron effective mass (m^*) and μ_{opt} of the AZO films were estimated. By comparing μ_{opt} and μ_{Hall}, we have studied the variation in the scattering mechanism causing thickness dependence of μ_{Hall}. The variation in the scattering mechanism was correlated with the development of the crystal structure with different substrate temperatures.

2. Experiments

AZO thin films were fabricated on c-sapphire substrates via PLD. The chamber was evacuated to a base pressure of 5.9×10^{-6} Torr. An Al-doped ZnO target (98 wt% ZnO+2 wt% Al_2O_3) with diameter of 1 in. and thickness of 1/8 of an inch was used for the study. A 248 nm-wavelength KrF laser (Lambda Physik LPX Pro) was focused onto the target at a repetition rate of 2 Hz. The laser energy density was kept at 1.0 J/cm^2. The oxygen pressure was fixed at 50 mTorr. The substrate was placed at a distance of 60 mm from the target. The target was rotated continuously during the laser ablation. In this study, AZO thin films were fabricated at a substrate temperature between 200 and 300 °C.

After deposition, the structural and optical properties of the AZO thin films were characterized by X-Ray diffraction (XRD-PANalytical), micro-PL -Raman setup (HR UV 800) and spectroscopic ellipsometry (VUV and UV to NIR-VASE, J.A. Wollam Co., Inc., USA). The electrical properties were measured by van der Pauw Hall measurement system (Ecopia-HMS 5000).

2.1. Modeling of dielectric function

Spectroscopic ellipsometry (SE) is a nondestructive tool for analyzing thin films. Measuring at several angles of incidence over a wide spectral range produces a wealth of information about the sample. The measured ellipsometric values are Ψ and Δ, which are determined from the ratio of the amplitude reflection coefficients r_p and r_s respectively for p- and s-polarizations with the following relationship [32]:

$$\rho = \tan\Psi \exp(-i\Delta) = \frac{r_p}{r_s}; \quad \Delta = \delta_p - \delta_s \tag{1}$$

We fit ellipsometric and transmission spectra using suitable dielectric function models for ZnO: Al and by adjusting the model-parameters it is possible to minimize deviations between the calculated and experimental data. During the fitting, the VWASE32 software determines the mean square error (MSE) and minimization of MSE has been done using a Levenberg–Marquardt algorithm [33,34]. MSE is a sum of the squares of the differences between the measured and calculated data weighted by the standard deviation of the data. In addition, it is necessary to weight the transmission modeling to avoid the overestimation of Ψ- and Δ-data with respect to the transmission data. In our model, we divide the ZnO:Al film into two layers: the surface roughness layer and ZnO:Al bulk layer. The most commonly used models for fitting the ellipsometric spectra in UV-visible range for TCOs are Lorentz, [35–37] Cauchy, [38] and Sellmeier [39] models. The latter two are simplified forms of the Lorentz representation and are suitable for any material in its transparent region [32]. Tauc–Lorentz [40] and Forouhi–Bloomer [41] models are more rarely applied. For the free carrier absorption in the near infrared region (NIR), the Drude model is commonly employed for TCOs and metals. It is used to analyze either the SE or transmission data [42,43]. Cauchy and Drude models for fitting the in situ ellipsometry data have already been reported in the literature for Al doped ZnO films [44]. In this work also we use a combined Cauchy–Drude models for the photon energy ranges from 0.6 to 6.5 eV.

3. Result and discussion

Fig. 1 shows XRD pattern of Al doped ZnO (AZO) films. It exhibits two diffraction peaks corresponding to (002) and (004) planes. The Al peak cannot be seen, because only 2 wt% Al_2O_3 was doped. They show the characteristic hexagonal ZnO wurtzite structure with the *c*-axis being perpendicular to the substrate plane [45]. The FWHM of the (002) diffraction peaks are 0.231 for 200 °C and 0.148 for 300 °C. For evaluating the mean grain size (D)

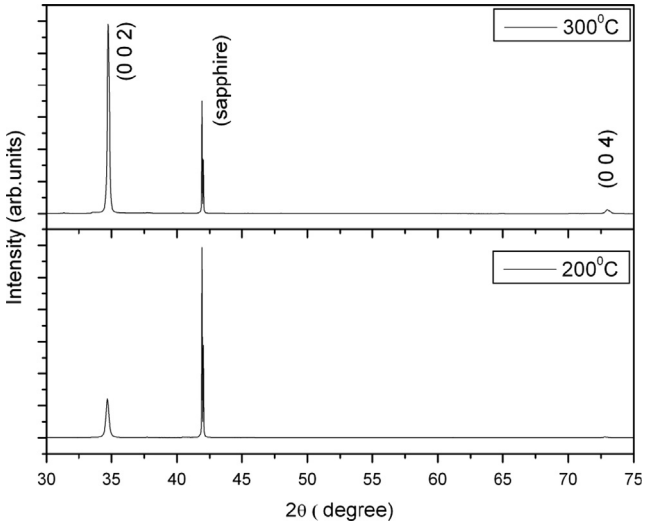

Fig. 1. X-ray diffraction pattern of AZO films.

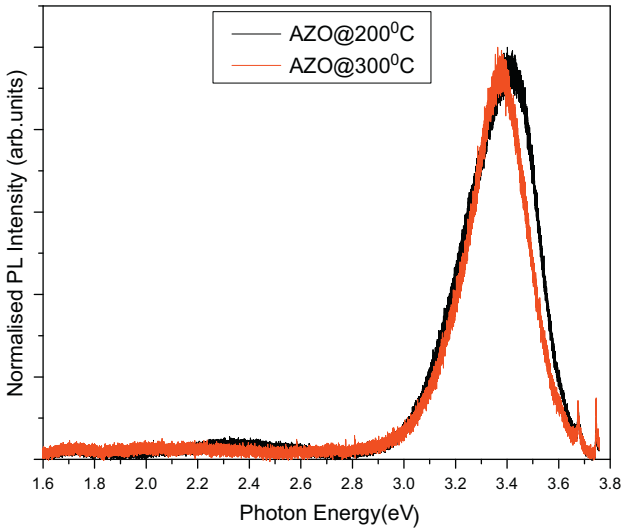

Fig. 2. Micro-PL spectra of AZO films.

of the film based on the XRD results, we have applied the Scherrer formula [46]

$$\text{Grain Size } (D) = \frac{0.9\lambda}{\beta \cos \theta} \quad (2)$$

where λ, β, θ represent the X-ray wavelength (1.5406 Å), the FWHM of the (002) diffraction peak for AZO, and the Bragg diffraction angle, respectively. Generally the FWHM of the (002) diffraction peak is inversely proportional to the grain size of the film. We have calculated the mean grain size of the AZO thin film which are 36.027 nm for 200 °C and 56.247 nm for 300 °C.

Fig. 2 shows the micro-photoluminescence (μ-PL) spectrum of AZO film excited by 325 nm UV light from a He–Cd laser at room temperature. The room temperature μ-PL spectra has been taken for two different substrate temperatures (200 and 300 °C) which contain a strong UV emission (peaked at 3.409 and 3.379 eV) and a very weak, broad band spread from 2.1 to 2.8 eV. The UV emission originates from the excitonic recombination, corresponding to the near-band-edge emission of the film.

Liu et al (2007 and 2009) reported [47,48] that it is very interesting to note that all the AZO films with different substrate temperatures observe only ultraviolet emission without noticeable deep level emissions (DLE). As a result, the deep level emission centered around 2.30 eV is expected for the AZO film. Because Al ions exists in Al^{3+} and Zn ions in Zn^{2+}, when Al element is doped in ZnO, Al ions will consume residual O ions and decrease the concentration of O_i defects (yellow luminescence) in AZO films. A strong UV emission with very slight or without deep-level emission were observed from the AZO films with different substrate temperatures [49].

The effect of Al doping in ZnO film has been examined by micro-Raman spectroscopy using a 325 nm laser. For all the samples, multiphonon peaks range from 200 to 3000 cm^{-1} are observed. The multi-phonon scattering processes have been observed in doped ZnO thin films [50] and Fig. 3 shows the typical resonant Raman spectra. The Raman spectrum of AZO film consists of three sharp lines at 565.5, 1130.98 and 1711 cm^{-1}, which arise from the emission of 1, 2 and 3 longitudinal optical (A_1LO) phonons of the AZO wurtzite structure. This result is consistent with the previously reported Raman shift of ZnO bulk crystal and thin films [50–53]. For AZO thin films, a typical Raman spectrum has been observed up to 3rd order. The second order E_2(low) peak observed at around 206 cm^{-1} is due to the substitution of the Al atom on the zinc site of the lattice. The strong peaks at about 443 and 435 cm^{-1} are assigned to the E_2(high) mode of AZO films with substrate temperatures at 200 and 300 °C, respectively, which is a Raman active mode in the wurtzite crystal structure. The strong E_2(high) mode indicates very good crystallanity [50]. A very small Raman active peak appear near 315 cm^{-1} can be assigned to the E_2(high)–E_2(low), where the E_2(high) mode is emitted and E_2(low) mode is absorbed. The incorporation of impurities in the host lattice generally can introduce forbidden vibrational modes (FVMs) which are observed in the Raman spectra. A possible physical mechanism for explaining FVMs is that defects induced by impurities break the translational symmetry of the crystal, thus

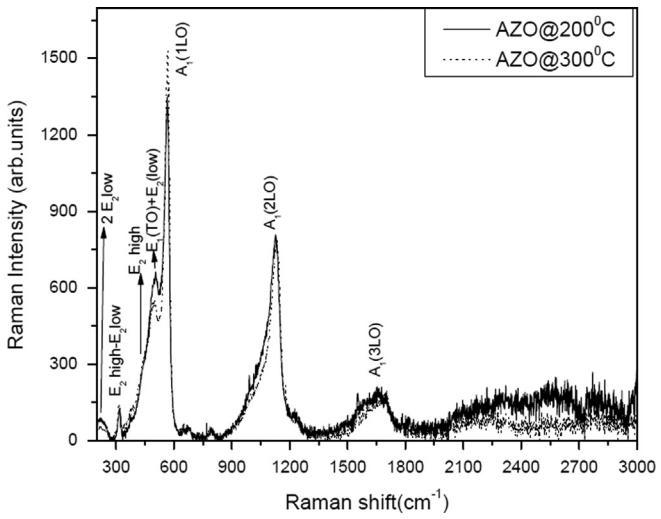

Fig. 3. Micro-Raman spectra of AZO films.

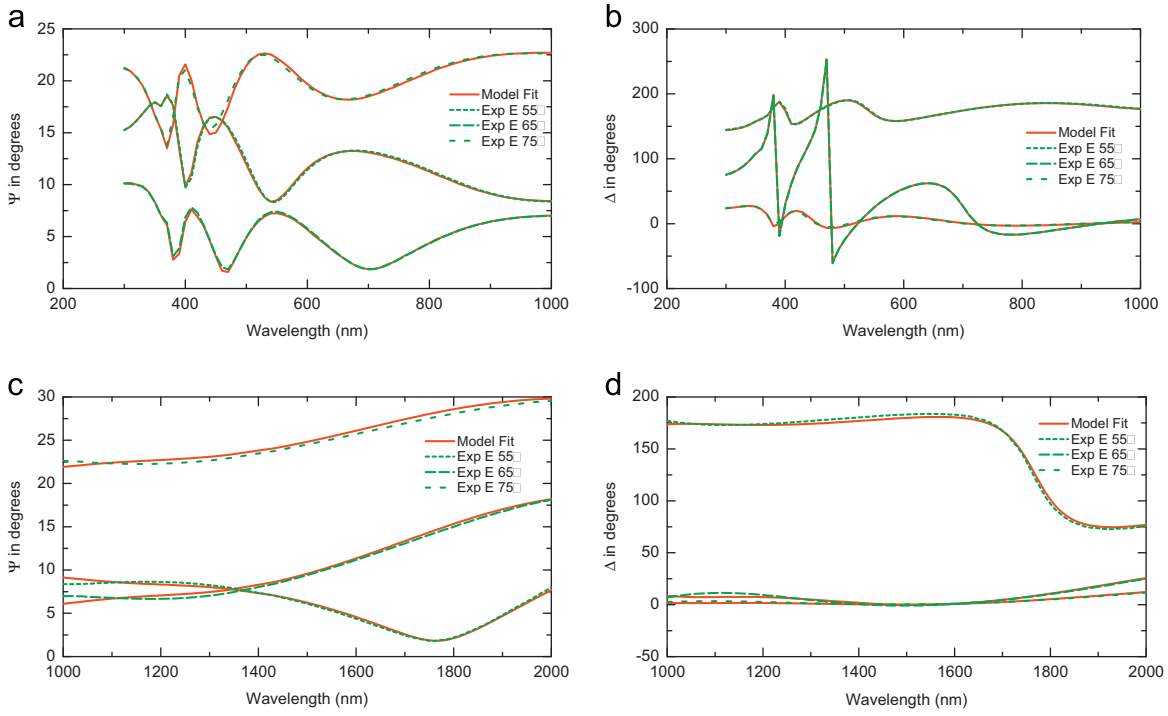

Fig. 4. (a, b, c and d). Ellipsometric spectra of the Al doped ZnO film grown at substrate temperature 300 °C.

Table 1
Cauchy–Drude model parameters and electrical properties of AZO films.

Fitting parameter	Substrate temperature (°C)	
	200	300
Film thickness (nm)	301.73	303.065
Surface roughness (nm)	6.010	5.281
Cauchy constant *A*	1.8434	1.8673
Cauchy constant *B*	0.0113	0.125
MSE	3.789	3.491
Drude model parameters		
(i) Carrier concentration (cm^{-3})	1.2909×10^{20}	1.221×10^{20}
(ii) Mobility ($cm^2\ V^{-1}\ S^{-1}$)	13.223	14.991
(iii) Resistivity (Ω cm)	3.6565×10^{-3}	3.47×10^{-3}
(iv) electron effective mass (m^*)	0.2953	0.2839
(v) Tau (fs)	2.2202	2.4195
MSE	11.03	9.084
Hall effect		
(i) Carrier Concentration (cm^{-3})	1.52×10^{20}	1.35×10^{20}
(ii) Mobility ($cm^2\ V^{-1}\ S^{-1}$)	11.353	13.697
(iii) Resistivity (Ω cm)	3.67×10^{-3}	3.57×10^{-3}

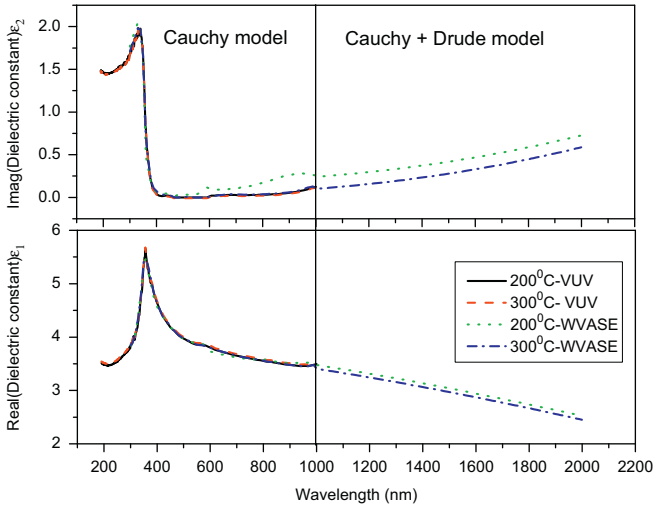

Fig. 5. Optical dielectric constants of the AZO films determined from Cauchy (190–1000 nm) and Drude (1000–2000 nm) model for substrate temperature at 200 °C and 300 °C.

relaxing the momentum conservation and hence leading to the scattering of phonons with the wave vectors far from the Brillouin zone center [54]. The new FVM assigned as $E_1(TO)+E_2(low)$ at about 498 cm^{-1} has been clearly observed in the Raman spectra of AZO films.

Fig. 4(a, b, c and d) shows typical Ψ, Δ spectrum measured at three different angles (55, 65 and 75°) of incidence for the AZO film with thickness of ~300 nm. The best-fit curves to the spectral data using Cauchy model and Drude model analysis, are also shown as solid lines in figures. Here the fitting is performed for the Drude model where the photon energy (wavelength) range is from 0.62 eV (2000 nm) to 1.24 eV (1000 nm) and for the Cauchy model it is between 1.24 eV (1000 nm) and 4.2 eV (300 nm) there is a good agreement between the experimental data and the calculated results. The result indicates that there is definite absorption which arises due to the free electrons over the entire visible range.

The surface roughness, thickness of the AZO layer *d*AZO, *A*, *B*, *N*, μ_{opt}, and m^* are used to fit in the Cauchy and Drude model of the SE analysis. The best-fit parameters obtained are summarized in Table 1.

Fig. 5 shows the optical dielectric constants ($\varepsilon=\varepsilon_1+i\varepsilon_2$) of AZO films determined by fitting the ellipsometric parameters. A strong peak in the spectra near the band gap is attributed to the free exciton absorption. In the longer wavelength region, we see an evidence for the free carrier absorption in AZO films. The changes of optical dielectric constants of the films with different substrate temperatures in the wavelength range of 190 nm–1000 nm are noticeable. The imaginary part of optical dielectric constant reduces to nearly zero for wavelengths between 400 nm and 1000 nm but it increases above 1000 nm due to the free-carrier absorption [44].

The electrical properties are investigated for Al doped ZnO thin films. Here aluminum acts as an effective donor, which substitute for zinc increasing significantly the concentration of free carriers in ZnO. With the increase of the substrate temperature, the resistivity of the AZO film decreases while mobility increases from 11.3 to 13.69 $cm^2\ V^{-1}\ s^{-1}$ [47–49]. Comparison of the calculated values of N_{opt} and μ_{opt} from SE with N_{Hall} and μ_{Hall} determined by Hall measurements are available in Table 1. It can be seen that N_{Hall} is slightly higher than N_{opt}, but μ_{Hall} is lower than μ_{opt}, find a fruitful validity of our analyses agreeing with the previous reported values [44].

4. Conclusion

Structural, electrical and optical properties of Al doped ZnO (AZO) films deposited at different substrate temperatures on *c*-plane sapphire substrates by pulser laser deposition were investigated to explore the possibility of producing transparent conductive oxide films through a simple low-cost process. It was observed that the AZO films were grown with *c*-axis preferred orientations without any degradation of ZnO wurtzite structure. Micro-PL spectra clearly indicate a strong UV emission of the samples. The new FVM assigned as $E_1(TO)+E_2(low)$ at about 498 cm^{-1} was clearly observed in the Raman spectra of AZO films. We further investigated the optical carrier concentration and mobility from the SE analyses using the Drude model. The results of the SE analysis have an excellent agreement with Hall measurements. This is an important result for the future, potential applications.

Acknowledgments

This research was supported by Academia Sinica, National Chiao Tung University, and National Science Council, Taiwan, Republic of China under the Grant number NSC-101–2112-M-001–024-MY3.

References

[1] H. Ohta, H. Hosono, Mater. Today 7 (2004) 42.
[2] H. Kim, A. Pique, J.S. Horwitz, H. Mattoussi, H. Murata, Z.H. Kafafi, D.B. Chrisey, Appl. Phys. Lett. 74 (1999) 3444.
[3] T. Minami, MRS Bull. 25 (2000) 38;
M. Chen, Z.L. Pei, C. Sun, J. Gong, R.F. Huang, L.S. Wen, Mater. Sci. Eng. B 85 (2001) 212.
[4] D.G. Thomas, J. Phys. Chem. Solids 15 (1960) 86.
[5] S.M. Park, T. Ikegami, K. Ebihara, Jpn. J. Appl. Phys. 44 (2005) 8027.
[6] S.M. Park, T. Ikegami, K. Ebihara, P.K. Shin, Appl. Surf. Sci. 253 (2006) 1522.
[7] K. Matsubara, P. Fons, K. Iwata, A. Yamada, K. Sakurai, H. Tampo, S. Niki, Thin Solid Films 431–432 (2003) 369.
[8] S.W. Shin, G.H. Lee, A.V. Moholkar, J.H. Moon, G.S. Heo, T.W. Kim, J.H. Kim, J. Y. Lee, J. Cryst. Growth 322 (2011) 51.
[9] J. Hu, R.G. Gordon, J. Appl. Phys. 71 (1992) 880.
[10] S. Oda, H. Tokunaga, N. Kitajima, J. Hanna, I. Shimizu, H. Kokado, Jpn. J. Appl. Phys. Part 1 24 (1985) 1607.
[11] T. Minami, K. Oohashi, S. Takata, T. Mouri, N. Ogawa, Thin Solid Films 193/194 (1990) 721.

[12] Y. Igasaki, H. Saito, J. Appl. Phys. 70 (1991) 3613.
[13] T. Minami, H. Sato, H. Natnto, S. Takata, Jpn. J. Appl. Phys. Part 2 24 (1985) L781.
[14] A.F. Aktaruzzaman, G.L. Sharma, L.K. Malhotra, Thin Solid Films 198 (1991) 67.
[15] D. Goyal, P. Solanki, B. Maranthe, M. Takwale, V. Bhide, Jpn. J. Appl. Phys. Part 1 31 (1992) 361.
[16] A. Suzuki, T. Matsushita, N. Wada, Y. Sakamoto, M. Okuda, Jpn. J. Appl. Phys. Part 2 35 (1996) L56.
[17] M. Hiramatsu, K. Imaeda, N. Horio, M. Nawata, J. Vac. Sci. Technol. A 16 (1998) 669.
[18] D.B. Chrisey, G.K. Hubler, Pulsed Laser Deposition of Thin Films, Wiley, New York, 1994.
[19] H. Kim, A. Piqué, J.S. Horwitz, H. Mattoussi, H. Murata, Z.H. Kafafi, D.B. Chrisey, Appl. Phys. Lett. 74 (1999) 3444.
[20] A. Geivandov, I. Kasianova, E. Kharatiyan, A. Lazarev, P. Lazarev, S. Palto, EuroDisplay Digest, Crysoptix KK, Moscow, Russia26.
[21] Q.H. Li, D. Zhu, W. Liu, Y. Liu, X.C. Ma, Appl. Surf. Sci. 254 (2008) 2922.
[22] F.K. Shan, Z.F. Liu, G.X. Liu, B.C. Shin, Y.S. Yu, J. Korean Phys. Soc. 44 (2004) 1215.
[23] N. Ehrmann, R.R. Koch, Thin Solid Films 519 (2010) 1475.
[24] R. Noriega, J. Rivnay, L. Goris, D. Kälblein, H. Klauk, K. Kern, L.M. Thompson, A.C. Palke, J.F. Stebbins, J.R. Jokisaari, G. Kusinski, A. Salleo, J. Appl. Phys. 107 (2010) 074312.
[25] K.M. Lin, K.-Y. Chou, P.-M. Chen, Phys. Status Solidi C 5 (2008) 3128.
[26] P.L. Washington, H.C. Ong, J.Y. Dai, R.P.H. Chang, Appl. Phys. Lett. 72 (1998) 25.
[27] M. Rebien, W. Henrion, M. Bär, Ch.H. Fischer, Appl. Phys. Lett., 80, 19.
[28] F.K. Shan, G.X. Liu, W.J. Lee, G.H. Lee, I.S. Kim, B.C. Shin, Y.C. Kim, J. Cryst. Growth 277 (2005) 284.
[29] E. Dumont, B. Dugnoille, S. Bienfait, Thin Solid Films 353 (1999) 93.
[30] C. Bundesmann, N. Ashkenov, M. Schubert, A. Rahm, H.V. Wenckstern, E.M. Kaidashev, M. Lorenz, M. Grundmann, Thin Solid Films 455 (2004) 161.
[31] G. Serrano, N. Koshizaki, T. Sasaki, G. MMontes, U. Pal, J. Mater. Res. 16 (2001) 3554.
[32] H. Fujiwara, Spectroscopic Ellipsometry: Principles and Applications, John Wiley Sons Ltd., Chichester, 2007.
[33] W.H. Press, S.A. Teukolsky, W.T. Vetterling, B.P. Flannery, Numerical Recipes in C++: The Art of Scientific Computing, 2nd ed., Cambridge University Press, Cambridge, UK, 2002.
[34] J.A. Woollam Co., Inc., Guide to Using WVase32.
[35] M. Losurdo, Thin Solid Films 455–456 (2004) 301.
[36] L.J. Meng, E. Crossan, A. Voronov, F. Placido, Thin Solid Films 422 (2002) 80.
[37] Y.S. Jung, Thin Solid Films 467 (2004) 36.
[38] Y.C. Liu, S.K. Tung, J.H. Hsieh, J. Cryst. Growth 287 (2006) 105.
[39] Z.F. Liu, F.K. Shan, Y.X. Li, B.C. Shin, Y.S. Yu, J. Cryst. Growth 259 (2003) 130.
[40] H. Fujiwara, M. Kondo, Phys. Rev. B 71 (2005) 075109.
[41] K. Zhang, A.R. Forouhi, I. Bloomer, J. Vac. Sci. Technol. A 17 (1999) 1843.
[42] S. Brehme, F. Fenske, W. Fuhs, E. Nebauer, M. Poschenrieder, B. Selle, I. Sieber, Thin Solid Films 342 (1999) 167.
[43] E. Langereis, S.B.S. Heil, M.C.M. van de Sanden, W.M.M. Kessels, J. Appl. Phys. 100 (2006) 023534.
[44] I Volintiru, M. creatore, M.C.M. van de Sanden, J. Appl. Phys. 103 (2008) 033704.
[45] S. Choopum, R.D. Vispute, W. Zoch, A. Balsamo, R.P. Sharma, T. Venkatesan, A. Iliadis, D.C. Lock, Appl. Phys. Lett. 75 (1999) 394.
[46] B.D. Cullity, Elements of X-ray diffraction, 2nd ed., Addison-Wesley, Reading, MA, 1978.
[47] Y. Liu, J. Lian, Appl. Surf. Sci. 253 (2007) 372.
[48] Y. Liu, Q. Li, H. Shao, J. Alloys Compd. 485 (2009) 529.
[49] E.L. Papadopoulou, M. Varda, K. Kouroupis-Agalou, M. Androulidaki, E. Chikoidze, P. Galtierd, G. Huyberechtsd, E. Aperathitis, Thin Solid Films 516 (2008) 8141.
[50] R. Thangavel, R.S. Moirangthem, W.S. Lee, Y.C. Chang, P.K. Wei, J. Kumar, J. Raman Spectrosc. 41 (2010) 1304.
[51] X.T. Zhang, Y.C. Liu, L.G. Zhang, J.Y. Zhang, Y.M. Lu, D.Z. Shen, W. Xu, G.Z. Zhong, X.W. Fan, X.G. Kong, J. Appl. Phys. 92 (2002) 3293.
[52] J.F. Scott, Phys. Rev. B 2 (1970) 1209.
[53] J.G. Ma, Y.C. Liu, C.L. Shao, J.Y. Zhang, Y.M. Lu, D.Z. Shen, X.W. Fan, Phys. Rev. B 71 (2005) 125430.
[54] W.H. Weber, R. Merlin, Raman Scattering in Materials Science, Springer, Berlin21.